

Black Silicon IR Photodiode Supersaturated With Nitrogen by Femtosecond Laser Irradiation

Chun-Hao Li, Xue-Peng Wang, Ji-Hong Zhao, *Member, IEEE*, De-Zhong Zhang, Xin-Yue Yu, Xian-Bin Li, *Member, IEEE*, Jing Feng, *Member, IEEE*, Qi-Dai Chen, *Member, IEEE*, Sheng-Ping Ruan, and Hong-Bo Sun, *Fellow, IEEE*

Abstract—Micro-ripple and micro-bead structures are formed on a silicon (Si) surface after irradiation with femtosecond laser pulses in nitrogen (N₂) atmosphere. Simultaneously, supersaturated nitrogen (N) atoms, with a concentration above 10^{20} cm⁻³, are doped into the textured black Si layer via laser ablation. The N-doped Si exhibits strong below-bandgap infrared absorption from 1.1 to 2.5 μm, which remains nearly unchanged after annealing for 30 min at 873 K. The mechanism of this thermally stable infrared absorption is analyzed by first-principles calculations. According to the transmission electron microscopy results, multiple phases (including single crystalline, nanocrystalline, and amorphous phases) are observed in the laser-irradiated layer. Hall Effect measurements prove that N-dopants induce a low background free-carrier concentration ($\sim 1.67 \times 10^{16}$ cm⁻³). Finally, a Schottky-based bulk structure photodiode is made. This broadband photodiode exhibits good thermal stability and a photo-responsivity of 5.3 mA/W for 1.31 μm at a reverse bias of 10 V.

Index Terms—Femtosecond laser, nitrogen doping, black silicon, infrared detection, first-principles calculation.

I. INTRODUCTION

CURRENTLY, silicon (Si) material still plays an irreplaceable role in microelectronic industry. Si-based optoelectronic devices continue to attract strong interest of researchers and the commercial world due to their low cost and compatibility with the CMOS technology [1], [2]. However, the 1.07 eV bandgap of Si restricts its application for detecting near-infrared light beyond 1.1 μm, where the III-V and IV-VI groups semiconductors such as InGaAs, PbS, and PbSe are dominant materials for infrared detectors. To solve this problem, much effort has been dedicated to extending the absorption wavebands of Si by, for example, intentionally inducing structure defects in Si crystals by inert ion implantation

(He, B, Si, etc.) [3]–[5] or supersaturated doping of chalcogen elements (S, Se, and Te) by ion implantation or pulsed laser irradiation [6]–[8]. According to previous reports, most of the infrared photodetectors based on inert ion implantation are fiber-coupled single-point detectors with waveguide architecture. The fabrication process of these devices is restricted to temperatures below 575 K, since the infrared-absorption-related defects in these devices are unstable under thermal treatment. As to S-hyperdoped black Si (B-Si) irradiated by femtosecond (fs) laser pulses in SF₆, the sub-bandgap absorptance of hyperdoped Si increases to 90% for wavelengths from 1.1 to 2.5 μm [6], [7]. However, the high near-infrared absorption is also unstable after thermal annealing, which is a necessary process in optoelectronic device fabrication [7], [8]. In addition, donor states induced by S impurities in S-hyperdoped Si will result in a high background free-carrier concentration [9], [10], which can overwhelm the sub-bandgap photoelectric conversion signal and make detection of infrared light very difficult. Further efforts have been made to reduce the free-carrier concentration in hyperdoped Si via introducing gold (Au) as a self-compensation dopant. Au-hyperdoped Si is made by ion implantation and pulsed laser melting. Free-carrier concentration in this material is reduced via self-compensation of the Au-induced donor and acceptor energy levels [11]. However, Au-hyperdoped photodiodes do not exhibit high photo-responsivity (0.3 mA/W@−5 V for 1310 nm) due to their very low infrared absorptance (< 3%). In brief, to realize Si-based infrared detection, hyperdoped Si should at least meet the following two requirements: (i) a high and thermostable infrared absorption and (ii) a low free-carrier concentration.

In this paper, nitrogen (N) is chosen to be doped into Si substrates by fs laser irradiation due to the following advantages. Firstly, N impurities in Si crystal tend to form di-interstitial pairs (Ni–Ni), which are stable below 1073 K [12], [13]. Because of the neutral doping property of N dimers, the free-carrier concentration in N-doped B-Si should be low. Secondly, N impurities in Si crystal provide excellent flexibility in controlling oxygen precipitation [14]–[18], locking dislocations [19], controlling the vacancy concentration [20], and improving the mechanical strength [21]–[25]. Moreover, N-hyperdoped crystal Si shows stable sub-band absorption, which has been proved by first-principles calculations [42]. In the current work, non-toxic nitrogen (N₂) was chosen as the dopant for fabricating N-hyperdoped Si. In contrast to nitrogen trifluoride (NF₃) [26], it is very safe and environment-friendly. In addition, infrared photodiode devices based on

Manuscript received December 12, 2017; revised February 24, 2018; accepted March 2, 2018. Date of publication March 6, 2018; date of current version April 9, 2018. This work was supported in part by the National Key Research and Development Program of China and the National Natural Science Foundation of China (NSFC) under Grant 61775077, Grant 61590930, Grant 2017YFB1104300, Grant 61435005, and Grant 51335008. The associate editor coordinating the review of this paper and approving it for publication was Prof. Bhaskar Choubey. (Chun-Hao Li and Xue-Peng Wang contributed equally to this work.) (Corresponding authors: Ji-Hong Zhao; Hong-Bo Sun.)

C.-H. Li, X.-P. Wang, J.-H. Zhao, D. Z. Zhang, X. Y. Yu, X.-B. Li, J. Feng, Q.-D. Chen, and S.-P. Ruan are with the State Key Laboratory of Integrated Optoelectronics, College of Electronic Science and Engineering, Jilin University, Changchun 130012, China (e-mail: zhaojihong@jlu.edu.cn).

H.-B. Sun is with the State Key Laboratory of Integrated Optoelectronics, College of Electronic Science and Engineering, Jilin University, Changchun 130012, China, and also with the State Key Laboratory of Precision Measurement Technology and Instruments, Department of Precision Instrument, Tsinghua University, Beijing 100084, China (e-mail: hbsun@tsinghua.edu.cn).

Digital Object Identifier 10.1109/JSEN.2018.2812730

these materials have been systematically studied and can be well reproduced.

II. EXPERIMENTS AND THEORY

A. Fabrication of Black Si Samples and Photodiodes

Single-crystal Si (111) wafers (250 μm thick, n-type, $\rho > 1500 \Omega\cdot\text{cm}$) are cut into $15 \times 15 \text{ mm}^2$ squares and cleaned under ultrasonic bath in trichloroethylene, acetone, ethanol, and deionized water for 10 min respectively. Then these Si substrates are irradiated by fs laser pulses in a sealed chamber filled with N_2 under 0.1 MPa. Laser pulses are generated from a Ti:Sapphire fs laser amplifier (Spectra-Physics, 100 fs pulse duration, 800 nm wavelength, and 2.5 kHz repetition rate). The diameter of the laser spot incident onto the Si surface is 343 μm . To obtain large-area N-doped surface, the vacuum chamber is moved synchronously with a computer-controlled translation stage in the plane perpendicular to the direction of the incident laser beam. The translation path of the vacuum chamber has an S-shape, and the sweep speed is 2 mm/s. The displacement between two adjusted lines is 65 μm . The Si surface is irradiated by 1120 pulses at each point.

To fabricate N-doped Si photodiodes, $5 \times 5 \text{ mm}^2$ area of Si samples are fabricated under a laser fluence of 0.08 J/cm^2 . After laser-induced doping, N-doped samples are annealed at 873 K for 30 min and then dipped into a diluted HF solution (5%) to remove the native oxide layer from the Si surface. Afterwards, to produce an ohmic contact, metal aluminum (Al) is coated onto the N-doped side (front side) by thermal evaporation, followed by alloying the Al–Si interface through thermal annealing treatment (473 K, 1 min in Ar atmosphere). In addition, to ensure that the incident light can be well absorbed, the Al electrode is designed as a fingerlike grid illustrated in Fig. 5a and 5b. Then, an Au film is thermally evaporated onto the Si back surface that is not treated by the fs laser to form a Schottky contact.

B. Experimental Characterization Methods

Topography Characterization: Surface morphologies of the irradiated samples are obtained using a JSM-7500F field emission scanning electron microscope (SEM, JEOL, Japan). Transmission electron microscopy (TEM) micrographs and selected area diffraction (SAD) patterns are collected with JEM-2100F, JEOL TEM operated at 200 kV. The laser fluence used for sample fabrication is 0.05 J/cm^2 . To meet the standard of TEM measurements (the thickness of the detected layer should be smaller than 100 nm), N-doped reference samples are fabricated with a silicon-on-insulator (SOI) substrate (50 nm thick top Si, 375-nm-thick buried oxide) instead of the crystalline Si substrate. Then, the buried SiO_2 layer of the annealed (30 min at 873 K in Ar) reference sample is etched off by diluted HF (5%) at room temperature. As a result, scraps of the top layer (50 nm) on the N-doped Si are separated from the SOI substrate by chemical exfoliation and collected for TEM measurements. We note that all the collected B-Si scraps (top 50 nm) belong to the N-doped re-solidified layer, since the average melting depth of the Si substrate caused by the fs laser is about 500 nm (according to the secondary ion mass spectrometry (SIMS) result in Fig. 2a).

C. Optical and Electric Characterization

The total hemispherical (specular and diffuse) reflection (R) and transmission (T) of the samples are directly measured by a Shimadzu UV-3600 spectrophotometer equipped with an integrating sphere device (LISR-UV3100). The absorption (A) is calculated by the formula $A = (1 - R - T)$ in the range of 0.25–2.5 μm . The distribution profiles of the depth-dependent N concentration in the Si substrate are analyzed by SIMS. The instrument is equipped with a CAMECA 6F device using a 10 keV Cs^+ primary beam at an incident angle of 25 degrees with the surface normal. The detecting ozone area is $20 \times 20 \mu\text{m}^2$, and the total analyzed depth is more than 100 nm. The electrical properties (sheet carrier density and carrier mobility) are measured with an ACCENT HL5500PC Hall system at room temperature based on the Van der Pauw method. N-doped samples are fabricated on 15 mm square Si substrates under varying laser fluence (0.08, 0.15, 0.23, 0.30, and 0.38 J/cm^2) and annealed for 30 min at 873 K. Then, metal indium (In) electronic contacts of 1 mm diameter are deposited at the four corners of each B-Si sample. Afterwards, an alloying annealing process (1 min at 473 K) is applied to ensure a good ohmic contact between the metal In and the disorder layer. I–V properties of the N-doped infrared photodiodes are obtained by a Keithley 2400 sourcemeter. The response time of the devices is measured by an oscilloscope.

D. Theoretical Calculation

To provide a theoretical description, our calculation employs density functional theory [27] as implemented in the Vienna *ab initio* simulation package (VASP) code [28]. The electron–ion interaction is described by the projector augmented wave (PAW) pseudopotential [29]. We used the generalized gradient approximation (GGA) [30] for the exchange–correlation functional as proposed by Perdew–Burke–Ernzerhof (PBE) [31]. The samples of amorphous Si and N-doped amorphous Si (Si_{96}N_4) with 100 atoms are obtained through a melt–quench process by molecular dynamics (MD) simulations. Nosé thermostat [32] is used to control the temperature in the NVT canonical ensemble. The density of these samples is equal to the value obtained in previous experiments [33], [34]. The two samples are first heated at 3000 K for 3 ps, followed by quenching to 1900 K, and maintained for 6 ps in liquid phase. Finally, they are quenched to 300 K and then equilibrated for 9 ps. A time step of 1 fs and the Gamma point in Brillouin-zone sampling are used for the simulations. An energy cutoff of 400 eV is used. After optimizing the final amorphous structure, ϵ_2 is evaluated. For the property calculation, a higher energy cutoff of 520 eV is used.

III. RESULTS AND DISCUSSIONS

Four different samples are fabricated at different laser fluences of 0.05, 0.08, 0.23, and 0.30 J/cm^2 . As shown in Fig. 1a–d, the surface morphologies (viewed at 45° to the normal) of the N-doped B-Si samples are dependent on the laser fluence. When the laser fluence is below 0.08 J/cm^2 (Fig. 1a and b), ripple microstructures are formed. These ripple

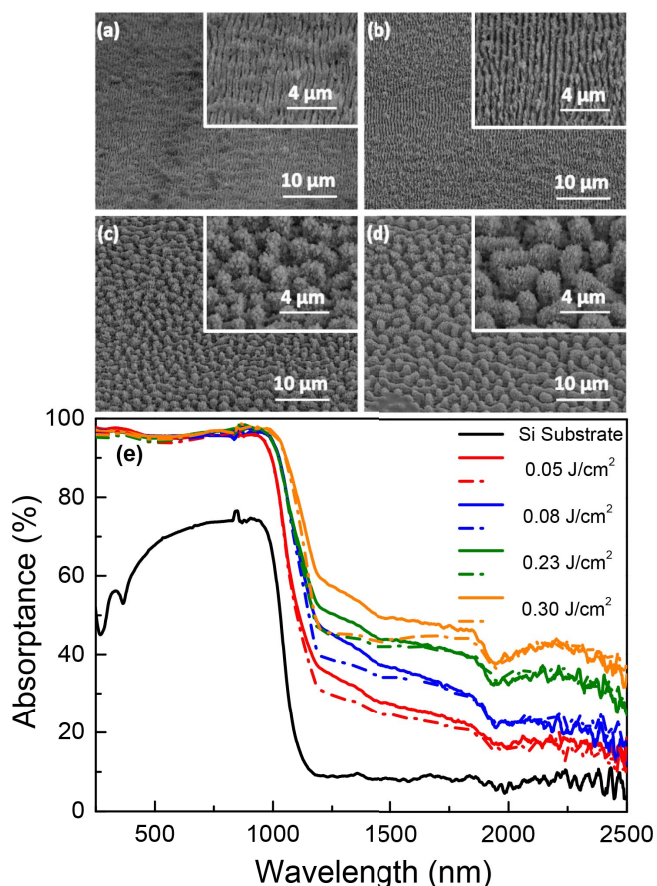


Fig. 1. (a)-(d) SEM images (tilt 45°) of nitrogen doped black silicon fabricated at different laser fluence: (a) 0.05 J/cm^2 , (b) 0.08 J/cm^2 , (c) 0.23 J/cm^2 , (d) 0.30 J/cm^2 , scale bars are $10 \mu\text{m}$ (mail panel) and $4 \mu\text{m}$ (inset) for (a)-(d), respectively; (e) The corresponding absorbance of four nitrogen doped samples and virgin silicon substrate. The solid lines and dash-dot lines represent the absorption of unannealed and annealed samples, respectively.

microstructures, with a period of $\sim 0.6 \mu\text{m}$, are parallel to the laser polarization [35]. When the laser fluence increases to more than 0.23 J/cm^2 (Fig. 1c and d), the ripple microstructures evolve to bead-like microstructures, which are $3\text{--}4 \mu\text{m}$ tall and separated by $3\text{--}4 \mu\text{m}$. Additionally, in the insets of Fig. 1c and d, nanoparticles with diameters of several hundred nanometers are observed on the bead-like micro-structured surface.

Fig. 1e shows the optical absorption spectra of the N-doped samples and Si substrate at wavelengths from 0.25 to $2.5 \mu\text{m}$. The small infrared absorption of the Si substrate is related to the imperfect baseline of the barium sulfate (BaSO_4) disk and the integrating sphere measurement system [38]. Compared to the absorbance of an unstructured Si substrate (the black line in Fig. 1e), the N-doped B-Si samples irradiated by fs laser pulses (solid colorlines) exhibit high broadband absorbance both above the bandgap ($0.25\text{--}1.1 \mu\text{m}$) and below the bandgap ($1.1\text{--}2.5 \mu\text{m}$). Here, the enhancement of absorbance above the bandgap can be attributed to the multi-reflections on the textured B-Si surface and the large contact area between the incident laser spot and micro-structured Si surface [36], [37]. The large below-bandgap absorbance ($20\text{--}50\%$) is caused by the structural defects related to the Urbach states and

the hyperdoped N atoms and further enhanced by the multi-reflection effect of the geometric structure. The below-bandgap absorption increases with laser fluence, since a higher laser fluence can induce stronger light trapping effect and dope more N atoms into the Si surface layer due to the deeper ablation. Annealing the B-Si samples at 873 K for 30 min in argon (Ar) retains the absorbance above the bandgap, while slightly decreasing the absorbance below the bandgap at the wavelengths of $1.1\text{--}1.7 \mu\text{m}$ (dash-dot lines in Fig. 1e). This reduction in the absorption corresponds to the elimination of the partial Urbach states, which are sensitive to high temperatures [8], [38]. However, the annealing process hardly affects the absorption at wavelengths of $1.7\text{--}2.5 \mu\text{m}$, which is determined by impurity doping. It should be mentioned that, even though the infrared absorbance of unannealed N-doped samples ($20\text{--}50\%$) is much lower than that of typical unannealed S-doped B-Si (more than 90%) [7], after thermal annealing, N-doped Si samples exhibit higher absorbance ($20\text{--}40\%$) than S-doped samples (20%). The large below-bandgap absorbance makes N-doped B-Si a promising material in the infrared optoelectronic field.

When the laser fluence is higher than the melting threshold of Si, doping of N atoms into the Si lattice can occur during the laser-induced melting and re-solidifying process. In order to measure the concentration distribution of N atoms in the textured Si surface layer, a SIMS measurement is performed. The concentration distributions of N impurities in B-Si (fabricated at 0.08 J/cm^2) before and after the annealing process are shown in Fig. 2a. After the laser doping, the N concentration in B-Si is about four orders of magnitude larger than the solid solubility of N atoms in Si [39]. The highest concentration of N impurities is $\sim 2.56 \times 10^{20} \text{ cm}^{-3}$ ($0.5 \text{ at.}\%$) at a depth of 68 nm for B-Si before annealing. However, after annealing, the highest concentration drops to $1.09 \times 10^{20} \text{ cm}^{-3}$ ($0.2 \text{ at.}\%$), and the corresponding depth changes to 130 nm . Furthermore, the N concentration in both samples stabilizes at a depth of $0.6\text{--}1.0 \mu\text{m}$, with the stabilized value of $\sim 6.0 \times 10^{17} \text{ cm}^{-3}$. The N concentration becomes constant after 500 nm , this may come from concentration lag effect of ultra-doped layer, which is caused by the fallback deposit and residual from spurting system. The inset figures are the N element images for three different doping depths, with the corresponding lateral resolution less than $1 \mu\text{m}$.

To determine the crystal structure of the N-doped layer modified by fs laser pulses, transmission electron microscopy (TEM) measurements are performed. Here, a B-Si sample (Fig. 2b) is fabricated with a laser fluence of 0.05 J/cm^2 and then annealed at 873 K for 30 min . The corresponding SAD pattern is shown in Fig. 2b. Magnified TEM images of a partial region (Fig. 2c, d, and e) indicate that three different phases (single crystalline, polycrystalline, and amorphous phase) exist in the N-doped layer. Actually, the re-solidified surface layer of the fs-laser-ablated Si is a disordered layer that consists of nanocrystalline Si grains and nanopores [40]. After thermal annealing, the amorphous phase tends to crystallize (Fig. 2c), although some amorphous phases still maintained (Fig. 2e). However, the SAD pattern in Fig. 2b indicates that

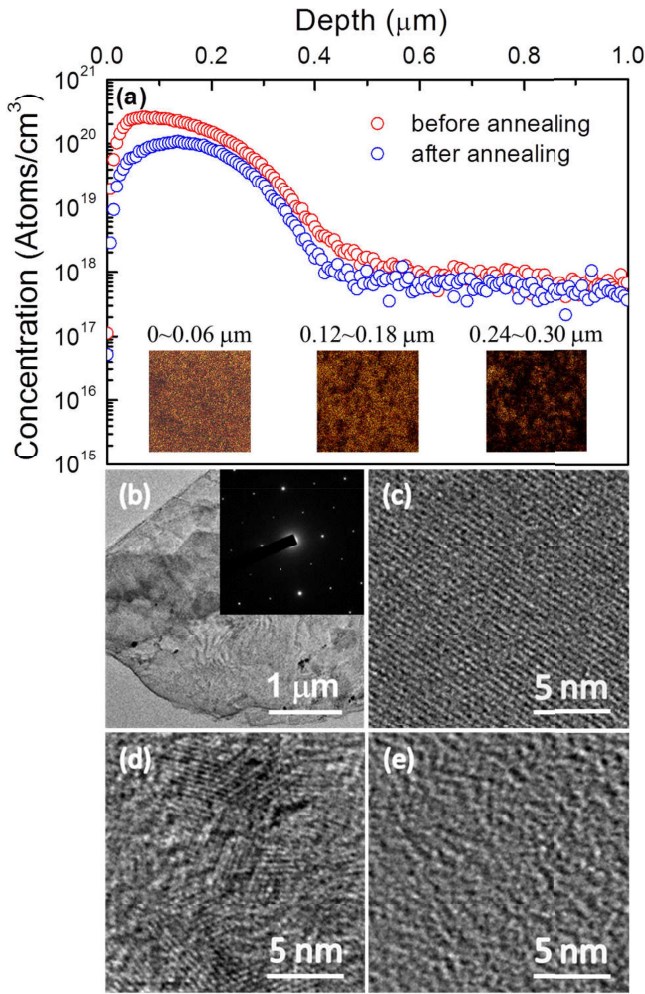


Fig. 2. (a) SIMS profiles of nitrogen doped silicon during a depth of $1 \mu\text{m}$; inserts are the dopant distribution in a specific area during three depths; (b)-(e) TEM images of the top 50 nm surface layer of nitrogen doped silicon samples, insert picture in (b) is the electronic diffraction pattern.

the N-doped layer has an obvious crystalline order, which may be because the amorphous phase is present between the nanocrystalline grains [41]. Overall, the N-doped surface is a complex disordered layer composed of multiple phases.

Next, the origin of the observed stable infrared absorption ($1.7\text{--}2.5 \mu\text{m}$) induced by supersaturated N dopants in N-doped Si should be clarified. To this end, theoretical calculations are performed to simulate the infrared absorption induced by N-doping. After fs laser irradiation, N impurities are doped into both the nanocrystalline and α -Si phases during the surface melting and re-solidifying process. Thus, the dopants in the α -Si phase should not be neglected. However, previous theoretical simulations for the sub-bandgap absorption of hyperdoped Si are mainly focused on impurity-doped crystalline Si [42], [43]. For a comprehensive study, we simulate the electronic structure of N-doped amorphous Si by first-principles calculations. Fig. 3a displays the atomic pictures. It is very clear that Si still has a coordination number of 4, while all the nitrogen has a coordination number of 3. Further, an average band angle distribution is shown to reveal their local configurations, see Fig. 3b. The bond angle distribution of Si is peaked at 109.5° , indicating the standard

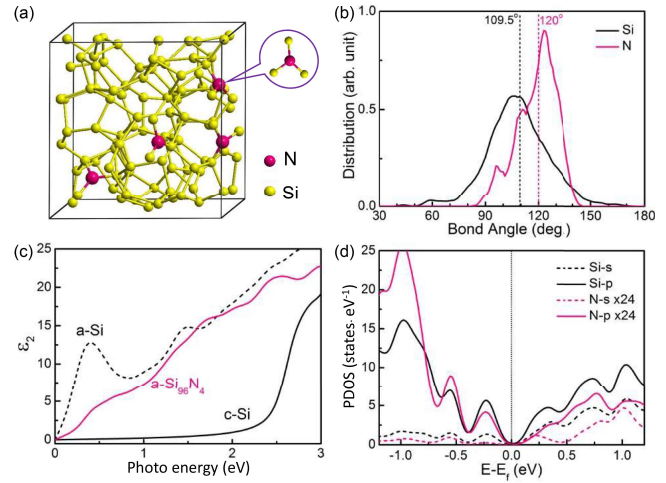


Fig. 3. First-principles study of N doped in amorphous Si. (a) Atomic picture and local configuration of N atom; (b) Bond angle distribution (per atom) for Si and N respectively. (c) The calculated imaginary part of permittivity for N doped amorphous Si ($a\text{-Si}_{96}\text{N}_4$), pure amorphous Si and crystalline Si. (d) Partial electronic density of states for Si (s, p) and N (s, p) electrons in $a\text{-Si}_{96}\text{N}_4$.

sp^3 hybridization motif. In contrast, the doped N atoms have an extra main peak at around 120° . Based on the N electronic configuration (s^2p^3), the three coordinated neighbors are naturally stratified according to the 8-N rule. However, owing to binding to silicon, here, we find not the pure p-bonding characteristic of N but a sp^2 -like local motif. In agreement with the experiment, the doped amorphous model has much stronger absorption (within the bandgap) than the crystalline Si (substrate) according to the calculated imaginary part of the permittivity (ϵ_2), see Fig. 3c. However, compared to pure amorphous Si without dopants, N-doped amorphous Si absorption in fact exhibits a certain degree of reduction. The partial density of states (PDOS) shown in Fig. 3d demonstrates that the N atom contributes few electronic states near the band edge or in the bandgap. Therefore, the N atom itself does not contribute directly to the infrared absorption, but its specific sp^2 -like robust motif can pin and stabilize the amorphous network in Si. Thus, N-doped samples can exhibit stable infrared absorption after thermal annealing.

The electronic properties of the annealed N-hyperdoped disordered layer are investigated by Hall Effect measurements based on the Van der Pauw technique. The measured results for the sheet carrier density and carrier mobility are shown in Fig. 4a. For all five B-Si samples, both the sheet carrier density and carrier mobility remain almost unchanged with the increase of the fabrication laser fluence. This is because the doping concentration of N impurities is mainly determined by the background N_2 pressure during the laser irradiation and melting process induced by fs laser ablation, so the N concentrations in all five samples are approximately the same [44]. Moreover, the sheet carrier electronic densities of all the N-doped Si samples are on the order of 10^{12} cm^{-2} , which is much larger than that of the original Si substrate ($\sim 10^{10} \text{ cm}^{-2}$), since a certain number of doped N atoms occupy positions in the Si lattice and form substitutional

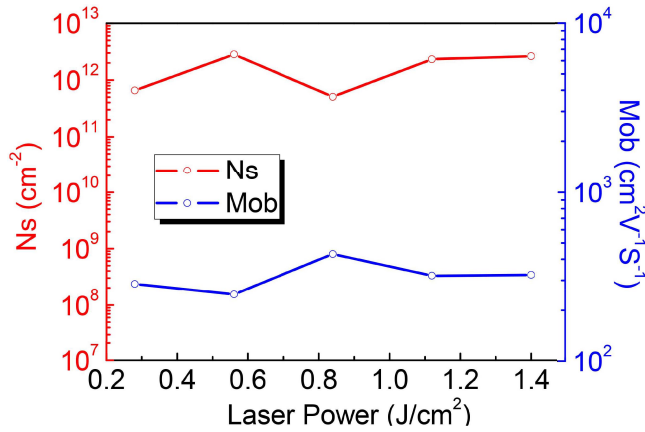


Fig. 4. Hall Effect measurements for sheet carrier concentration and carrier mobility of nitrogen doped silicon fabricated at different laser fluencies.

donor impurities. The carrier mobility of N-doped B-Si is on the order of $10^2 \text{ cm}^2\text{V}^{-1}\text{s}^{-1}$ (Fig. 4), which is an order of magnitude less than the value for the unstructured crystalline wafer ($1700 \text{ cm}^2\text{V}^{-1}\text{s}^{-1}$). The decrease of the carrier mobility can be attributed to the disorder structure in the surface layer and enhancement of impurity scattering.

Furthermore, the depth of the melting and resolidification layer of B-Si is about 500 nm [44], so the maximum bulk carrier density should be $\sim 1.67 \times 10^{16} \text{ cm}^{-3}$. This free-carrier concentration is much smaller than the average concentration of doped N atoms obtained from the SIMS measurement ($\sim 10^{19} \text{ cm}^{-3}$, Fig. 2a). It means that only about 0.2% of the doped N atoms possess electrical activity. In comparison to S-doped Si, where about 1~10% of the laser-doped S atoms are activated, the number of active atoms is much smaller in N-doped samples. This result again confirms that N in Si tends to form neutral doping dimers other than free-carrier donors.

Based on the described results, N-doped B-Si samples turn out to be a promising candidate for making infrared photodetectors due to two outstanding advantages: the thermostable infrared absorption (from $1.1 \mu\text{m}$ to $2.5 \mu\text{m}$) and low free-carrier concentration. We then proceed to fabricate photodiodes from N-doped B-Si samples based on the Schottky barrier structure. Fig. 5a shows a schematic diagram of the completed device. An N-doped B-Si layer is fabricated on the front side of a Si substrate. A Schottky barrier is formed at the back side of the device at the Au-Si interface (for more details, see the experimental part). Current-voltage (*I-V*) characteristics of the N-doped B-Si photodiode are shown in Fig. 5c. At a reverse bias of 10 V, the device shows a low dark current density of 0.09 mA/cm^2 (dark line in Fig. 5c). The photocurrent (red line in Fig. 5c) clearly increases after illumination with $1.31 \mu\text{m}$ near-infrared light (5 mW laser diode), and the photo-responsivity is calculated to be 4.0 mA/W at -10 V , which is much larger than the photo-responsivity of a commercial PIN Si photodiode ($0.02 \text{ mA/W}@-10 \text{ V}$). For comparison, S-doped photodiodes are fabricated with the same device structure and experimental parameters. Similarly, the photo-responsivity of the S-doped photodiode ($0.6 \text{ mA/W}@-10 \text{ V}$ for $1.31 \mu\text{m}$) is much lower

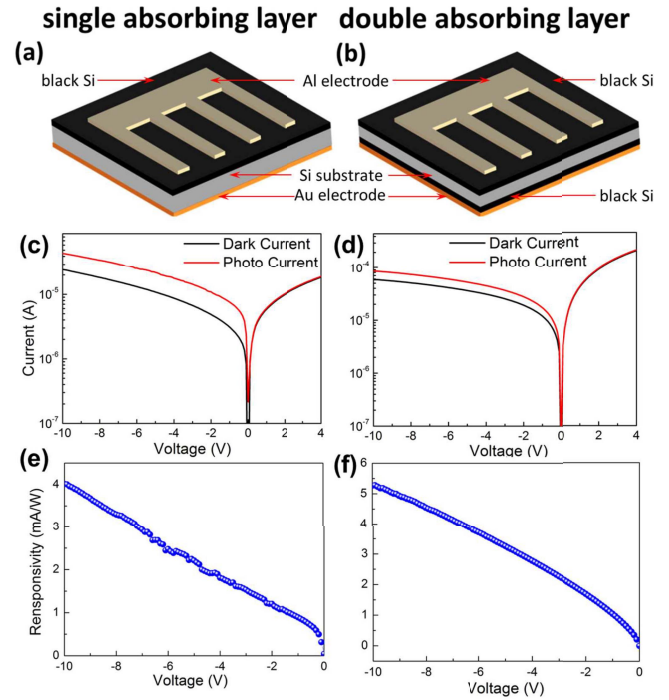


Fig. 5. (a) and (b) Two different schematic diagrams of nitrogen-doped silicon photodiodes. (c) and (d) The corresponding photo current and dark current vs voltage characteristics for the three photodiodes; (e) and (f) Corresponding responsivity vs reverse bias for the three photodiodes.

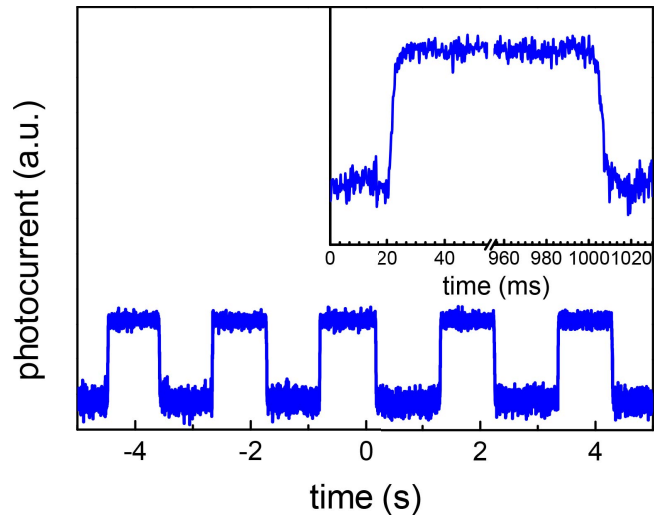


Fig. 6. Rise times and fall times of N-doped Si device with single-absorbing-layer.

than that of the N-doped one. Further, the time scales for the switching and the detectivity of the single-absorbing-layer Si device are evaluated. From a time-dependent measurement for the device (see Fig. 6), the response time and the rise and fall time scales are estimated to be 3.4 ms.

To increase the absorption of incident light, we introduce a double-absorbing-layer device structure (Fig. 5b). In this case, a Schottky contact is formed between the Au and N-doped Si back surface. Inevitably, this device has a relatively high dark current density ($0.23 \text{ mA/cm}^2@-10 \text{ V}$) due to the rough

Schottky contact surface. However, this device presents an obvious advantage, as shown by the dark line in Fig. 5d. At a reverse bias of 10 V, the photo-responsivity of the double-absorbing-layer device for 1.31 μm light is 5.3 mA/W; this responsivity is ~ 1.2 times higher than that of the single-absorbing-layer device. The higher responsivity of the double-absorbing-layer device indicates that the photogenerated $e-h$ pairs at the N-doped junction region contribute significantly to the good performance of the device. This is because the thickness of the implanted region of the double-absorbing-layer device is larger than that of the single-absorbing-layer device. The enhancement of the photo-responsivity is in accordance with the increase of the infrared absorptance, which is about 20% larger in double-absorbing-layer Si than in single-absorbing-layer Si because of a larger amount of photogenerated carriers for the double-absorbing-layer device.

To quantitatively determine the effect of the applied field on the $e-h$ pair splitting efficiency, the dependencies of the responsivity on the applied reverse voltage for two types of devices are given in Fig. 5e–f. From these dependencies, we can see that the responsivity increases rapidly and linearly with the increasing applied reverse voltage. This behavior implies that the photogenerated $e-h$ pair splitting efficiency would rise with the increasing applied electric field.

IV. CONCLUSIONS

In conclusion, N-hyperdoped B-Si is obtained by fs laser irradiation in N_2 atmosphere. Microstructures (ripples or beads) are observed on the Si surface layer after fs laser ablation. The N-doped layer exhibits strong below-bandgap absorption (20–50%) due to the Urbach-states-related defects and the hyperdoped N impurities. The latter contribution induces a thermal-insensitive infrared absorption in N-doped Si, because the N-atom-specific sp^2 -like robust motif can pin and stabilize the amorphous network in Si. Even though N atoms with a high concentration (above 10^{20} cm^{-3}) are doped into Si samples during the melting and re-solidifying process, only $\sim 0.2\%$ of these impurity atoms have electrical activity. Consequently, N-doped B-Si exhibits a low free-carrier concentration. At last, a Schottky-based bulk-structure photodiode is made from N-doped Si. The single-absorbing-layer photodiode has a low dark current density, good thermal stability, and a photo-responsivity of 4.0 mA/W for 1.31 μm at -10 V. Employing a double-absorbing-layer structure can increase the photo-responsivity to 5.3 mA/W at the same reverse bias.

ACKNOWLEDGMENT

The authors would like to thank Prof. Shan-Peng Wen for valuable help.

REFERENCES

- [1] Q. Xu, B. Schmidt, S. Pradhan, and M. Lipson, "Micrometre-scale silicon electro-optic modulator," *Nature*, vol. 435, p. 325–327, May 2005.
- [2] J. Leuthold, C. Koos, and W. Freude, "Nonlinear silicon photonics," *Nature Photon.*, vol. 4, pp. 535–544, Jul. 2010.
- [3] J. J. Ackert *et al.*, "High-speed detection at two micrometres with monolithic silicon photodiodes," *Nature Photon.*, vol. 9, pp. 393–396, May 2015.
- [4] Y. Liu, C. W. Chow, W. Y. Cheung, and H. K. Tsang, "In-line channel power monitor based on helium ion implantation in silicon-on-insulator waveguides," *IEEE Photon. Technol. Lett.*, vol. 18, no. 17, pp. 1882–1884, Sep. 1, 2006.
- [5] A. P. Knights, J. D. B. Bradley, S. H. Gou, and P. E. Jessop, "Silicon-on-insulator waveguide photodetector with self-ion-implantation-engineered-enhanced infrared response," *J. Vac. Sci. Technol. A, Vac. Surf. Films*, vol. 24, no. 3, p. 783, 2006.
- [6] T.-H. Her, R. J. Finlay, C. Wu, S. Deliwala, and E. Mazur, "Microstructuring of silicon with femtosecond laser pulses," *Appl. Phys. Lett.*, vol. 73, no. 12, p. 1673, 1998.
- [7] C. Wu *et al.*, "Near-unity below-band-gap absorption by microstructured silicon," *Appl. Phys. Lett.*, vol. 78, no. 13, p. 1850, 2001.
- [8] B. R. Tull, M. T. Winkler, and E. Mazur, "The role of diffusion in broadband infrared absorption in chalcogen-doped silicon," *Appl. Phys. A*, vol. 96, no. 2, pp. 327–334, 2009.
- [9] M. T. Winkler, D. Recht, M.-J. Sher, A. J. Said, E. Mazur, and M. J. Aziz, "Insulator-to-metal transition in sulfur-doped silicon," *Phys. Rev. Lett.*, vol. 106, p. 178701, Apr. 2011.
- [10] E. Ertekin *et al.*, "Insulator-to-metal transition in selenium-hyperdoped silicon: Observation and origin," *Phys. Rev. Lett.*, vol. 108, p. 026401, Jan. 2012.
- [11] J. P. Mailoa *et al.*, "Room-temperature sub-band gap optoelectronic response of hyperdoped silicon," *Nature Commun.*, vol. 5, p. 3011, Apr. 2014.
- [12] H. J. Stein, "Nitrogen in crystalline Si," in *Proc. Mater. Res. Soc. Symp.*, vol. 59, 1985, p. 523.
- [13] R. Jones, S. Öberg, F. B. Rasmussen, and B. B. Nielsen, "Identification of the dominant nitrogen defect in silicon," *Phys. Rev. Lett.*, vol. 72, p. 1882, Mar. 1994.
- [14] F. Shimura and R. S. Hockett, "Nitrogen effect on oxygen precipitation in Czochralski silicon," *Appl. Phys. Lett.*, vol. 48, no. 3, p. 224, 1986.
- [15] Q. Sun, K. H. Yao, H. C. Gatos, and J. Lagowski, "Effects of nitrogen on oxygen precipitation in silicon," *J. Appl. Phys.*, vol. 71, no. 8, p. 3760, 1992.
- [16] K. Aihara, H. Takeno, Y. Hayamizu, M. Tamatsuka, and T. Masui, "Enhanced nucleation of oxide precipitates during Czochralski silicon crystal growth with nitrogen doping," *J. Appl. Phys.*, vol. 88, no. 6, p. 3705, 2000.
- [17] K. Nakai *et al.*, "Oxygen precipitation in nitrogen-doped Czochralski-grown silicon crystals," *J. Appl. Phys.*, vol. 89, no. 8, p. 4301, 2001.
- [18] X. Yu, D. Yang, X. Ma, J. Yang, L. Li, and D. Que, "Grown-in defects in nitrogen-doped Czochralski silicon," *J. Appl. Phys.*, vol. 92, no. 1, p. 188, 2002.
- [19] J. D. Murphy *et al.*, "Nitrogen-doped silicon: Mechanical, transport and electrical properties," *ECS Trans.*, vol. 3, no. 4, pp. 239–253, 2006.
- [20] D. Gräf *et al.*, "Characterization of crystal quality by crystal originated particle delineation and the impact on the silicon wafer surface," *J. Electrochem. Soc.*, vol. 145, no. 1, pp. 275–284, 1998.
- [21] K. Sumino, I. Yonenaga, M. Imai, and T. Abe, "Effects of nitrogen on dislocation behavior and mechanical strength in silicon crystals," *J. Appl. Phys.*, vol. 54, no. 9, p. 5016, 1983.
- [22] G. Wang, D. Yang, D. Li, Q. Shui, J. Yang, and D. Que, "Mechanical strength of nitrogen-doped silicon single crystal investigated by three-point bending method," *Phys. B, Condens. Matter*, vols. 308–310, pp. 450–453, Dec. 2001.
- [23] A. Giannattasio, S. Senkader, R. J. Falster, and P. R. Wilshaw, "Dislocation locking by nitrogen impurities in FZ-silicon," *Phys. B, Condens. Matter*, vols. 340–342, pp. 996–1000, Dec. 2003.
- [24] V. I. Orlov, Y. L. Iunin, M. Badylevich, O. Lysytskiy, and H. Richter, "Influence of nitrogen on dislocation mobility in Czochralski silicon," *Solid State Phenom.*, vols. 95–96, pp. 465–472, Sep. 2004.
- [25] I. Yonenaga, "Nitrogen effects on generation and velocity of dislocations in Czochralski-grown silicon," *J. Appl. Phys.*, vol. 98, no. 2, p. 023517, 2005.
- [26] X. Dong *et al.*, "A nitrogen-hyperdoped silicon material formed by femtosecond laser irradiation," *Appl. Phys. Lett.*, vol. 104, p. 091907, Feb. 2014.
- [27] P. Hohenberg and W. Kohn, "Inhomogeneous electron gas," *Phys. Rev.*, vol. 136, p. B864, Nov. 1964.
- [28] G. Kresse and J. Furthmüller, "Efficient iterative schemes for *ab initio* total-energy calculations using a plane-wave basis set," *Phys. Rev. B, Condens. Matter*, vol. 54, p. 11169, Oct. 1996.
- [29] P. E. Blöchl, "Projector augmented-wave method," *Phys. Rev. B, Condens. Matter*, vol. 50, p. 17953, Dec. 1994.

- [30] J. P. Perdew and W. Yue, "Accurate and simple density functional for the electronic exchange energy: Generalized gradient approximation," *Phys. Rev. B, Condens. Matter*, vol. 33, no. 12, p. 8800, 1986.
- [31] J. P. Perdew, K. Burke, and M. Ernzerhof, "Generalized gradient approximation made simple," *Phys. Rev. Lett.*, vol. 77, no. 18, p. 3865, Oct. 1996.
- [32] N. Shuichi, "Constant temperature molecular dynamics methods," *Prog. Theor. Phys. Suppl.*, vol. 103, pp. 1–46, Jan. 1991.
- [33] J. S. Custer *et al.*, "Density of amorphous Si," *Appl. Phys. Lett.*, vol. 64, no. 4, p. 437, 1994.
- [34] X.-B. Li *et al.*, "Role of electronic excitation in the amorphization of Ge-Sb-Te alloys," *Phys. Rev. Lett.*, vol. 107, no. 1, p. 015501, Jun. 2011.
- [35] C. H. Crouch, J. E. Carey, M. Shen, E. Mazur, and F. Y. Génin, "Infrared absorption by sulfur-doped silicon formed by femtosecond laser irradiation," *Appl. Phys. A, Solids Surf.*, vol. 79, no. 7, pp. 1635–1641, 2004.
- [36] R. J. Younkin, "Surface studies and microstructure fabrication using femtosecond laser pulses," Ph.D. dissertation, Division Eng. Appl. Sci., Harvard Univ., Cambridge, MA, USA, 2001.
- [37] J. Yang *et al.*, "Design and fabrication of broadband ultralow reflectivity black Si surfaces by laser micro/nanoprocessing," *Light, Sci. Appl.*, vol. 3, p. e185, Jul. 2014.
- [38] M.-J. Sher and E. Mazur, "Intermediate band conduction in femtosecond-laser hyperdoped silicon," *Appl. Phys. Lett.*, vol. 105, no. 3, p. 032103, 2014.
- [39] Y. Yatsurugi, N. Akiyama, Y. Endo, and T. Nozaki, "Concentration, solubility, and equilibrium distribution coefficient of nitrogen and oxygen in semiconductor silicon," *J. Electrochem. Soc.*, vol. 120, no. 7, pp. 975–979, 1973.
- [40] J. E. Carey, III, "Femtosecond-laser microstructuring of silicon for novel optoelectronic devices," Ph.D. dissertation, Division Eng. Appl. Sci., Harvard Univ., Cambridge, MA, USA, 2004.
- [41] P. Keblinski, S. R. Phillpot, D. Wolf, and H. Gleiter, "Thermodynamically stable amorphous intergranular films in nanocrystalline silicon," *Phys. Lett. A*, vol. 226, p. 205–211, Feb. 1997.
- [42] Z. Zhu *et al.*, "Electronic band structure and sub-band-gap absorption of nitrogen hyperdoped silicon," *Sci. Rep.*, vol. 5, May 2015, Art. no. 10513.
- [43] H. Shao *et al.*, "Physical mechanisms for the unique optical properties of chalcogen-hyperdoped silicon," *Europhys. Lett.*, vol. 99, no. 4, p. 46005, 2012.
- [44] M.-J. Sher, M. Winkler, and E. Mazur, "Pulsed-laser hyperdoping and surface texturing for photovoltaics," *MRS Bull.*, vol. 36, no. 6, pp. 439–445, 2011.

Chun-Hao Li received the B.S. degree in microelectronics from the College of Electronic Science and Engineering, Jilin University, Changchun, China, in 2012. His current research interests include characterization of semiconductor surface and device.

Xue-Peng Wang received the B.S. degree in material physics from the College of Material Science and Engineering, Jilin University, Changchun, China, in 2012, and the M.S. degree in physical electronics from the College of Electronic Science and Engineering, Jilin University, in 2015. His current research interests include first-principles calculation on semiconductors.

Ji-Hong Zhao received the B.S. degree in microelectronics and the Ph.D. degree from the College of Electronic Science and Engineering, Jilin University, Changchun, China, in 2006 and 2011, respectively. She is currently an Associate Professor with Jilin University. Her current research interests include the analysis of properties of semiconductor surface by nonlinear optics, femtosecond laser micro- and nano-fabrication, and femtosecond laser-doping semiconductors.

De-Zhong Zhang received the B.S. degree in microelectronics from the College of Electronic Science and Engineering, Jilin University, Changchun, China, in 2013. His current research interests include photodetectors and solar cells.

Xin-Yue Yu received the B.S. degree in microelectronics from the College of Physics, Changchun University of Science and Technology, China, in 2015. She is currently pursuing the master's degree with the College of Electronic Science and Engineering, Jilin University, Changchun, China. She majors in microelectronics and solid state electronics. Her current research interests include semiconductor's doping by femtosecond laser irradiation.

Xian-Bin Li received the B.S., M.S., and Ph.D. degrees in microelectronics from Jilin University, China, in 2005, 2007, and 2010, respectively. He is currently an Associate Professor with the State Key Laboratory on Integrated Optoelectronics, College of Electronic Science and Engineering, and in-charge of the Research Branch of Computational Semiconductor Physics. His current research focuses on the key problems in microelectronics and optoelectronics with the first principles calculation, including phase-change memory physics, semiconductor defect physics, and 2-D semiconductor design.

Jing Feng received the B.S. and Ph.D. degrees in microelectronics and solid state electronics from Jilin University, Changchun, China, in 1997 and 2003, respectively. From 2003 to 2006, she was a Post-Doctoral Researcher with RIKEN, Japan. In 2006, she joined Jilin University, where she is currently a Professor with the State Key Laboratory on Integrated Optoelectronics, College of Electronic Science and Engineering. She has published over 100 scientific papers in academic journals. Her research interests include organic optoelectronic devices.

Qi-Dai Chen received the B.S. degree in physics from the University of Science and Technology of China, Hefei, China, in 1998, and the Ph.D. degree from the Institute of Physics, Chinese Academy of Sciences, Beijing, China, in 2004. He was a Post-Doctoral Research Associate at Osaka City University, Osaka, Japan, from 2005 to 2006. He is currently an Associate Professor with Jilin University, Changchun, China. His current research interests include laser microfabrication, ultrafast laser spectroscopy, photochemistry, and photophysics.

Sheng-Ping Ruan received the Ph.D. degree from the College of Electronic Science and Engineering, Jilin University, in 2001. He is currently a Full Professor with the College of Electronics Science and Engineering, Jilin University, and mainly devoting himself to the research of electronic functional materials and devices.

Hong-Bo Sun (F'17) received the B.S. and Ph.D. degrees from Jilin University, Changchun, China, in 1992 and 1996, respectively. He was a Post-Doctoral Researcher with the University of Tokushima, Japan, from 1996 to 2000, and then an Assistant Professor with the Department of Applied Physics, Osaka University, Japan. In 2005, he was promoted to Full Professor (Changjiang Scholar) at Jilin University. In 2017, he was with Tsinghua University. He has authored or co-authored over 400 scientific papers, which have been cited over 13000 times, with an H-factor of 57. His research interests include ultrafast optoelectronics, particularly on laser nanofabrication and ultrafast spectroscopy. In 2017 he was an OSA Fellow.